

# Energy-based Analysis of Biomolecular Pathways

Peter J. Gawthrop\*<sup>1</sup> and Edmund J. Crampin<sup>2</sup>

<sup>1</sup> Systems Biology Laboratory, Department of Biomedical Engineering, Melbourne School of Engineering, University of Melbourne, Victoria 3010, Australia.

Department of Electrical and Electronic Engineering, Melbourne School of Engineering, University of Melbourne, Victoria 3010, Australia.

<sup>2</sup> Systems Biology Laboratory, Melbourne School of Engineering, University of Melbourne, Victoria 3010, Australia.

School of Mathematics and Statistics, University of Melbourne, Victoria 3010, Australia.

School of Medicine, University of Melbourne, Victoria 3010, Australia.

ARC Centre of Excellence in Convergent Bio-Nano Science, Melbourne School of Engineering, University of Melbourne, Victoria 3010, Australia.

October 7, 2018

## Abstract

Decomposition of biomolecular reaction networks into pathways is a powerful approach to the analysis of metabolic and signalling networks. Current approaches based on analysis of the stoichiometric matrix reveal information about steady-state mass flows (reaction rates) through the network. In this work we show how pathway analysis of biomolecular networks can be extended using an energy-based approach to provide information about energy flows through the network. This energy-based approach is developed using the engineering-inspired bond graph methodology to represent biomolecular reaction networks. The approach is introduced using glycolysis as an exemplar; and is then applied to analyse the efficiency of free energy transduction in a biomolecular cycle model of a transporter protein (Sodium-Glucose Transport Protein 1, SGLT1). The overall aim of our work is to present a framework for modelling and analysis of biomolecular reactions and processes which considers energy flows and losses as well as mass transport.

---

\*Corresponding author. [peter.gawthrop@unimelb.edu.au](mailto:peter.gawthrop@unimelb.edu.au)

# Contents

<b>1</b>	<b>Introduction</b>	<b>3</b>
<b>2</b>	<b>Energy-based Reaction Analysis</b>	<b>4</b>
<b>3</b>	<b>Stoichiometric Pathway Analysis</b>	<b>7</b>
<b>4</b>	<b>Energy-based Pathway Analysis</b>	<b>8</b>
<b>5</b>	<b>Example: Free Energy Transduction and Biomolecular Cycles</b>	<b>11</b>
<b>6</b>	<b>Example: The Sodium-Glucose Transport Protein 1 (SGLT1)</b>	<b>18</b>
<b>7</b>	<b>Conclusion</b>	<b>20</b>
<b>A</b>	<b>A Short Introduction to Bond Graph Modelling</b>	<b>27</b>
<b>B</b>	<b>A Short Introduction to Systems Biology</b>	<b>30</b>

# 1 Introduction

The term “pathway analysis” is used very broadly in systems biology to describe several quite distinct approaches to the analysis of biomolecular networks [1–3] and often the definition of a “pathway” is somewhat nebulous. In this work we are concerned with those pathways defined in terms of the stoichiometric analysis of biomolecular reaction networks [4–8]; in particular, the null space<sup>1</sup> of an appropriate stoichiometric matrix is used to identify the pathways of a biomolecular network. Two alternative concepts of pathways: *elementary modes* and *extreme pathways* are compared and contrasted by Papin et al. [3]. Computational issues are considered by Schuster and Hilgetag [9], Pfeiffer et al. [10], Schilling et al. [11] and Schuster et al. [12]. A brief introduction to the relevant concepts appears in Appendix B.

These approaches have proven to be very useful in determining network properties and emergent behaviour of biomolecular reaction networks in terms of the pathway “building blocks” of these networks. However, these approaches are solely focused on *mass* flows of biomolecular reaction networks. However, to date, little attention has been given to the identification and analysis of pathways in the context of *energy* flows in biomolecular reaction networks. This paper extends the pathway concept to include such energy flows using an engineering-inspired method: the bond graph.

Like engineering systems, living systems are subject to the laws of physics in general and the laws of thermodynamics in particular [13–17]. This fact gives the opportunity of applying engineering science to the modelling, analysis and understanding of living systems. The bond graph method of Paynter [18] is one such energy-based engineering approach [19–24] which has been extended to include chemical systems [20, 25], biological systems [26] and biomolecular systems [27–32]. A brief introduction to the bond graph approach appears in Appendix A.

Applying the bond graph method to modelling biomolecular pathways moves the focus from mass flow to energy flow. Hence this paper brings together stoichiometric pathway analysis with energy based bond graph analysis to identify the pathways of steady-state free energy transduction in biomolecular networks. Although the bond graph approach is well-established in the field of engineering, and the stoichiometric pathway analysis approach well-established in the field of biochemical analysis, they have not hitherto been brought together. As illustrated in the Sodium-Glucose Transport Protein example of § 6, this interdisciplinary synthesis gives new insight into the energetic behaviour of living systems.

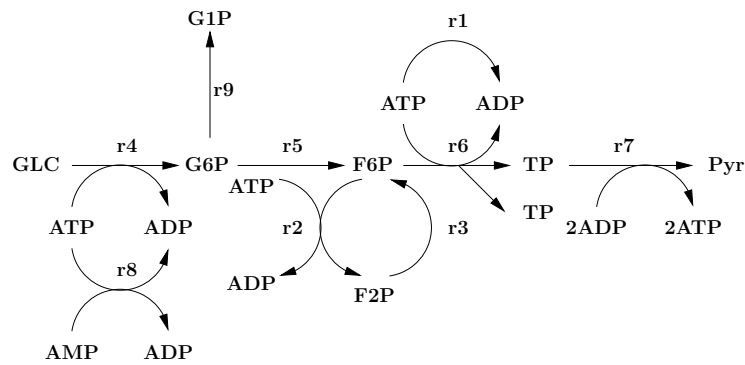
§ 2 introduces the bond graph approach to pathway analysis using glycolysis as an exemplar. As a preliminary to the energy-based approach, § 3 discusses the stoichiometric approach to pathway analysis. § 4 combines the energy-based reaction analysis of §2 with the stoichiometric pathway analysis of §3 to give an energy-based pathway analysis of biomolecular systems. § 5 looks at the generic biomolecular cycle transporter model of Hill [14] focusing on the energy transduction aspects; in particular, a two-pathway decomposition provides insight into free-energy dissipation and efficiency. § 6 uses this two-pathway decomposition to look at a particular transporter – The Sodium-Glucose Transport Protein 1 (SGLT1) – using parameters drawn from the experimental results of Eskandari et al. [33]. § 7 draws some conclusions and indicates fu-

---

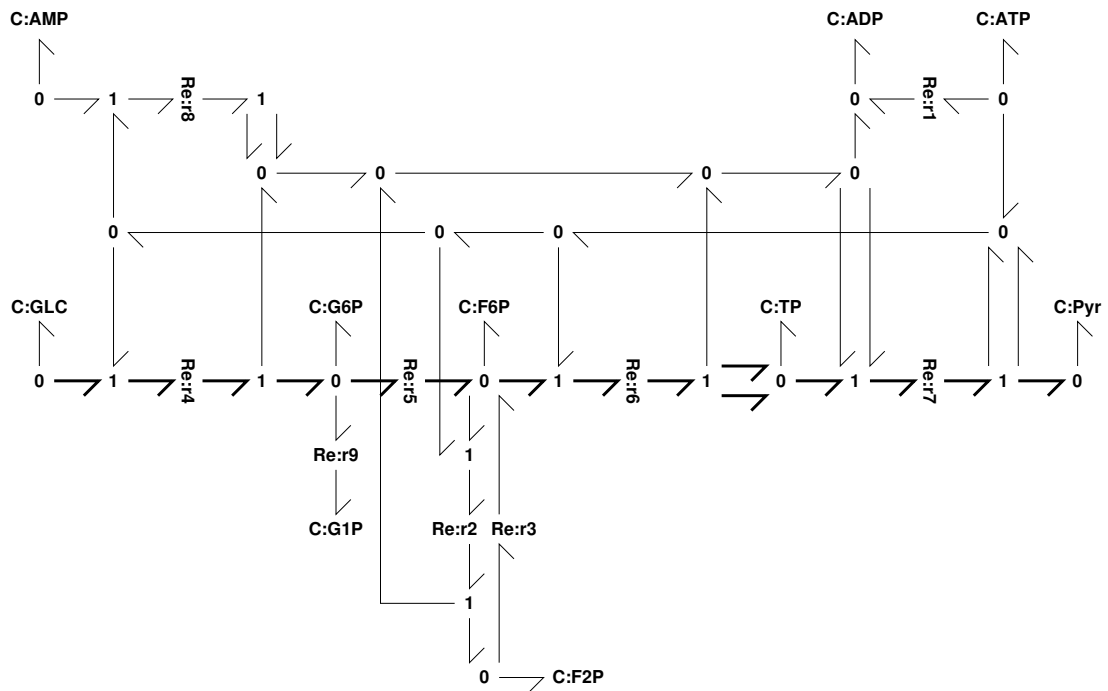
<sup>1</sup>The mathematical concept of a null space is given a biological interpretation in Appendix B.

ture research directions. Appendix A provides a short introduction to those features of the bond graph approach necessary to understand this paper and Appendix B similarly introduces systems biology. The complete equations describing the examples are given in the Supplementary Material.

## 2 Energy-based Reaction Analysis



(a) Biomolecular reaction diagram of the glycolysis pathway

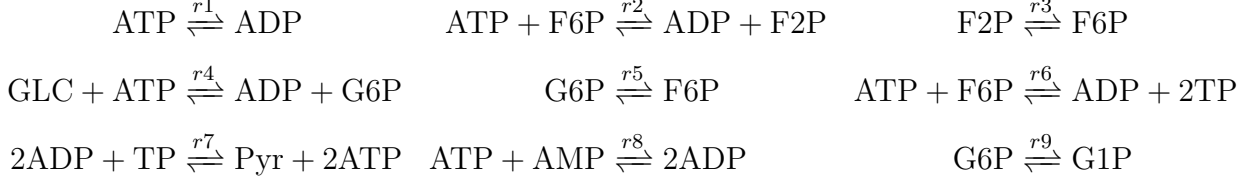


(b) Bond Graph representation of the biomolecular pathway shown above

Figure 1: Glycolysis example from Heinrich and Schuster [5].

As reviewed in the Introduction, and as discussed by Gawthrop and Crampin [29, 31] and

Appendix A, chemical equations can be written in the form of bond graphs to enable energy-based analysis. As an introductory and illustrative example, the glycolysis example from the seminal book of Heinrich and Schuster [5, Figure 3.4] has the following chemical equations:



These equations can be represented by the biomolecular reaction diagram of Figure 1(a) or the equivalent bond graph of Figure 1(b). Briefly, each reaction is represented by an **Re** component and each species by a **C** component. The (Gibbs) energy flows are represented by bonds  $\rightarrow$  which carry both chemical potential and molar flow. Bonds are connected by **0** junctions which imply a common chemical potential on each bond and **1** junctions which imply a common molar flow on each bond. **C** components store, **Re** components dissipate and bonds and junctions transmit Gibbs energy. Further details are given in Appendix A and references [29–32].

Closed biomolecular systems are described in stoichiometric form as:

$$\dot{X} = NV \quad (1)$$

where  $X$  is the  $n_X \times 1$  system state,  $V$  the  $n_V \times 1$  vector of reaction flows and  $N$  is the  $n_X \times n_V$  stoichiometric matrix which can be derived from the bond graph representation [29, 32]. In the case of the example of Figure 1:

$$X = \begin{pmatrix} x_{GLC} \\ x_{Pyr} \\ x_{ATP} \\ x_{ADP} \\ x_{G1P} \\ x_{G6P} \\ x_{F6P} \\ x_{TP} \\ x_{F2P} \\ x_{AMP} \end{pmatrix}, \quad N = \begin{pmatrix} 0 & 0 & 0 & -1 & 0 & 0 & 0 & 0 & 0 \\ 0 & 0 & 0 & 0 & 0 & 0 & 1 & 0 & 0 \\ -1 & -1 & 0 & -1 & 0 & -1 & 2 & -1 & 0 \\ 1 & 1 & 0 & 1 & 0 & 1 & -2 & 2 & 0 \\ 0 & 0 & 0 & 0 & 0 & 0 & 0 & 0 & 1 \\ 0 & 0 & 0 & 1 & -1 & 0 & 0 & 0 & -1 \\ 0 & -1 & 1 & 0 & 1 & -1 & 0 & 0 & 0 \\ 0 & 0 & 0 & 0 & 0 & 2 & -1 & 0 & 0 \\ 0 & 1 & -1 & 0 & 0 & 0 & 0 & 0 & 0 \\ 0 & 0 & 0 & 0 & 0 & 0 & 0 & -1 & 0 \end{pmatrix}, \quad V = \begin{pmatrix} v_{r1} \\ v_{r2} \\ v_{r3} \\ v_{r4} \\ v_{r5} \\ v_{r6} \\ v_{r7} \\ v_{r8} \\ v_{r9} \end{pmatrix} \quad (2)$$

In the case of mass-action kinetics [8], the reaction flows are generated by the formula:

$$V = \kappa \left( \exp \frac{A^f}{RT} - \exp \frac{A^r}{RT} \right) \quad (3)$$

where  $A^f$  and  $A^r$  are the forward and reverse<sup>2</sup> reaction affinities. As discussed by Gawthrop and Crampin [29, 31], these affinities are given by:

$$A^f = N^{fT} \mu, \quad A^r = N^{rT} \mu \quad (4)$$

<sup>2</sup>The terms “forward” and “reverse” often correspond to “substrate” and “product” respectively or “input” and “output” respectively; they are used here for consistency with previous work, to avoid ambiguity and to recognise that reactions may be reversible.

where  $^T$  indicates matrix transpose and  $\mu$  is the (vector of) chemical potentials where the  $i$ th element is a logarithmic function of the  $i$ th element  $x_i$  of  $X$ :

$$\mu_i = RT \ln K_i x_i \quad (5)$$

where  $K_i$  is a species-specific positive constant.  $N^f$  and  $N^r$  are the forward and reverse stoichiometric matrices, and conservation of energy requires that:

$$-N^f + N^r = N \quad (6)$$

By definition, all stoichiometric parameters, that is the elements  $N_{ij}^f$  of  $N^f$  and the elements  $N_{ij}^r$  of  $N^r$  have the following properties:

$$N_{ij}^f \text{ is integer} \quad N_{ij}^f \geq 0 \quad N_{ij}^r \text{ is integer} \quad N_{ij}^r \geq 0 \quad (7)$$

As discussed by Gawthrop and Crampin [31], open biomolecular systems can be described and analysed using the notion of *chemostats* [34, 31]. Chemostats have two biomolecular interpretations:

1. one or more species are fixed to give a constant concentration (for example under a specific experimental protocol); this implies that an appropriate external flow is applied to balance the internal flow of the species.
2. as a **C** component with a fixed state imposed on a model in order to analyse its properties [30].

Additionally, in the context of a control systems analysis, the chemostat can be used as an ideal feedback controller, applied to species to be fixed with setpoint as the fixed concentration and control signal an external flow.

When chemostats are present, the reaction flows are determined by the dynamic part of the stoichiometric matrix. In this case the stoichiometric matrix  $N$  can be decomposed as the sum of two matrices [31]: the *chemostatic* stoichiometric matrix  $N^{cs}$  and the *chemodynamic* stoichiometric matrix  $N^{cd}$  where  $N = N^{cs} + N^{cd}$  and:

$$N^{cs} = I^{cs} N \quad N^{cd} = I^{cd} N \quad I_{ii}^{cs} = \begin{cases} 1 & \text{if } i \in \mathcal{I}^{cs} \\ 0 & \text{if } i \notin \mathcal{I}^{cs} \end{cases} \quad I_{ii}^{cd} = \begin{cases} 0 & \text{if } i \in \mathcal{I}^{cs} \\ 1 & \text{if } i \notin \mathcal{I}^{cs} \end{cases} \quad (8)$$

Note that  $N^{cd}$  is the same as  $N$  except that the *rows* corresponding to the chemostat variables are set to zero. In this case  $N^{cd}$  is given by  $N$  of Equation (2) with rows 1–4 set to zero.

With these definitions, an open system can be expressed as

$$\dot{X} = N^{cd} V \quad (9)$$

The stoichiometric properties of  $N^{cd}$ , rather than  $N$ , determine system properties when chemostats are present. Using equation (8),  $\dot{X}$  in equation (9) can also be written as:

$$\dot{X} = NV - N^{cs}V = NV + V^s \quad \text{where } V^s = -N^{cs}V \quad (10)$$

$V^s$  can be interpreted as the external flows required to hold the chemostat states constant. The reaction flows are given by the same formulae (3) & (4) as closed systems.

### 3 Stoichiometric Pathway Analysis

As discussed in the textbooks [4–8] and Appendix B, the (non-unique)  $n_V \times n_P$  null-space matrix  $K_p$  of the open system stoichiometric matrix  $N^{cd}$  has the property that

$$N^{cd}K_p = 0 \quad \text{where } n_P = n_V - r \quad (11)$$

and  $r$  is the rank of  $N$ . Furthermore, if the reaction flows  $V$  are constrained in terms of the  $n_P$  pathway flows  $V_p$  as

$$V = K_p V_p \quad (12)$$

then substituting Equation (12) into Equation (1) and using Equation (11) implies that  $\dot{X} = 0$ . This is significant because the biomolecular system of equation (1) may be in a steady state for any choice of  $V_p$ .

As mentioned above,  $K_p$  is not unique: there are many possible approaches to choosing  $K_p$  such that Equation (11) holds. As discussed by, for example, Pfeiffer et al. [10],  $K_p$  can be computed in such a way as to give useful features such as integer entities and maximal number of zero elements; moreover, if all reactions are irreversible, the columns of  $K_p$  must correspond to a convex space<sup>3</sup>. As discussed in §4, the analysis of this paper requires that all elements  $K_{pij}$  of  $K_p$  must satisfy the same conditions as those on  $N_{ij}^f$  and  $N_{ij}^r$  (7), namely:

$$K_{pij} \text{ is integer} \quad K_{pij} \geq 0 \quad (13)$$

For this reason,  $K_p$  is referred to as the *positive-pathway matrix* (PPM) in the sequel. This does *not* imply that reactions are assumed to be irreversible; however, one approach to generating such a  $K_p$  is using software such as `metatool` [10] as if all reactions were irreversible.

In the case of the glycolysis system of Figure 1, Heinrich and Schuster [5] choose the chemostats to be: GLC, Pyr, ATP and ADP. Using the algorithm of Pfeiffer et al. [10]<sup>4</sup>,  $K_p$  for the glycolysis system of Figure 1 was computed as

$$K_p = \begin{pmatrix} 1 & 0 & 0 \\ 0 & 1 & 0 \\ 0 & 1 & 0 \\ 0 & 0 & 1 \\ 0 & 0 & 1 \\ 0 & 0 & 1 \\ 0 & 0 & 2 \\ 0 & 0 & 0 \\ 0 & 0 & 0 \end{pmatrix} \quad (14)$$

The pathways corresponding to the three columns of  $K_p$ , (referring to Figure 1(a)), are:  $\{r1\}$ ,  $\{r2 \ r3\}$  and  $\{r4 \ r5 \ r6 \ 2r7\}$ . The latter pathway is marked on the bond graph of 1(b) using

<sup>3</sup>This is related to the classical Cone Lemma [35, Chap. 10].

<sup>4</sup>The Octave [36] version of `metatool` from <http://penguin.biologie.uni-jena.de/bioinformatik/networks/metatool/metatool5.0/metatool5.0.html> was used.

bold bonds. As pointed out by Heinrich and Schuster [5], these three pathways are independent insofar as they have no reactions in common; as will be seen in the rest of this section and in the examples of §5 and §6, this is not always the case.

The number of pathways, and their independence, not only depend on the network structure, but also on the choice of chemostats. To illustrate this point, consider the same glycolysis system of Figure 1, but choose an additional chemostat to be G1P. In this case,  $K_p$  is given by:

$$K_p = \begin{pmatrix} 1 & 0 & 0 & 0 \\ 0 & 1 & 0 & 0 \\ 0 & 1 & 0 & 0 \\ 0 & 0 & 1 & 1 \\ 0 & 0 & 1 & 0 \\ 0 & 0 & 1 & 0 \\ 0 & 0 & 2 & 0 \\ 0 & 0 & 0 & 0 \\ 0 & 0 & 0 & 1 \end{pmatrix} \quad (15)$$

The first three columns of Equation (15) are identical to the three columns of Equation (14). The fourth column corresponds to the additional pathway  $\{r4 \ r9\}$ , which shares reaction  $r4$  with the pathway  $\{r4 \ r5 \ r6 \ 2r7\}$  corresponding to the third column of Equations (15) and (14).

## 4 Energy-based Pathway Analysis

This section combines the energy-based reaction analysis of §2 with the stoichiometric pathway analysis of §3 to give an energy-based pathway analysis of biomolecular systems.

As discussed by Gawthrop and Crampin [29, 31], Equations (1), (4) and (6) can be summarised by the diagram of Figure 2(a). The key point here is that the energy flow from the reaction components represented by the vectors of covariables  $A^r$  and  $V$  is transformed without energy loss by  $\mathcal{TF} : N^r$  into the energy flow to the  $\mathcal{C}$  components represented by the vectors of covariables  $\mu$  and  $\dot{X}^r$  and the energy flow from the  $\mathcal{C}$  components represented by the vectors of covariables  $\mu$  and  $\dot{X}^f$  is transformed without energy loss by  $\mathcal{TF} : N^f$  into the energy flow to reaction components represented by the vectors of covariables  $A^f$  and  $V$ . Dissipation of energy occurs at the reaction components  $\mathcal{R}e$ . The challenge for an energy-based pathway analysis is to determine the energy flow associated with each pathway.

The key result of the stoichiometric pathway analysis summarised in §3 is Equation (12) relating the pathway flow vector  $V_p$  to the reaction flow vector  $V$  by  $V = K_p V_p$ . To bring this result into the energy domain, we define the forward and reverse pathway affinities  $A_p^f$  and  $A_p^r$ , and the pathway affinity  $A_p$ , as:

$$A_p^f = K_p^T A^f \quad A_p^r = K_p^T A^r \quad A_p = A_p^f - A_p^r = K_p^T (A^f - A^r) = K_p^T A \quad (16)$$



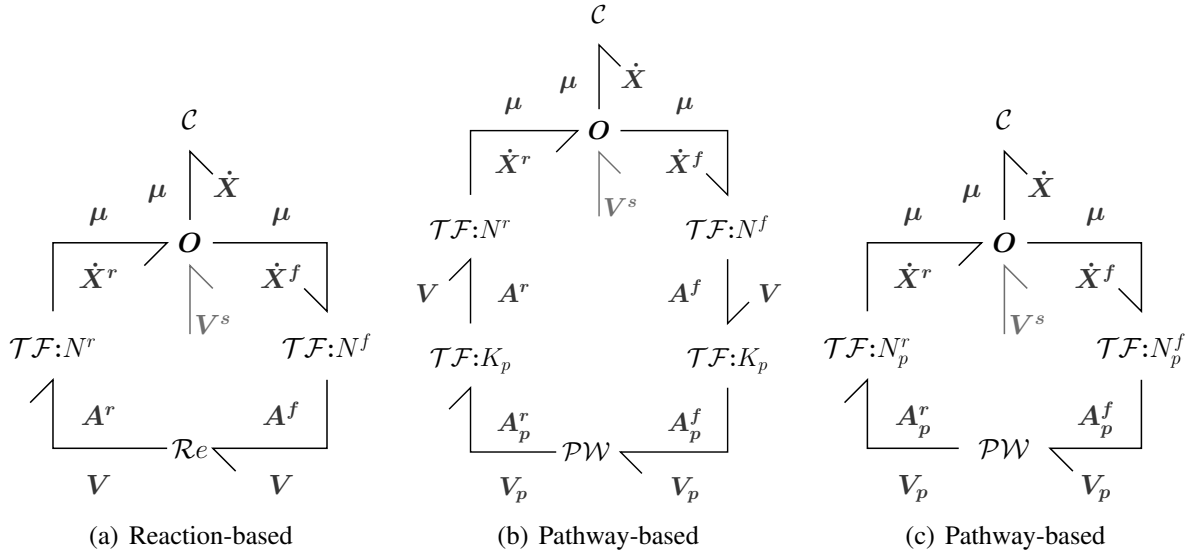


Figure 2: Energy-based analysis. (a) Reaction-based system [31]. The bond symbols  $\rightarrow$  correspond to *vectors* of bonds;  $\mathcal{C}$ ,  $\mathcal{R}e$  and  $\mathcal{O}$  correspond to arrays of **C**, **Re** and **O** components; the two  $\mathcal{TF}$  components represent the intervening junction structure comprising bonds, **O** and **1** junctions and **TF** components.  $N^f$  and  $N^r$  are the forward and reverse stoichiometric matrices.  $V^s$  represents the chemostatic flows. (b) The positive-pathway matrix  $K_p$  maps the  $n_p$  positive-pathway flows  $V_p$  onto the  $n_V$  reaction flows  $V$  and also maps the  $n_V$  reaction affinities onto the  $n_p$  positive-pathway affinities.  $\mathcal{PW}$  conceptually represents the non-linear function generating the steady-state positive-pathway flows in terms of the positive-pathway affinities; unlike  $\mathcal{R}e$ , it does *not* have a diagonal structure. (c)  $\mathcal{TF}$  components have been merged using  $N_p^f = N^f K_p$  and  $N_p^r = N^r K_p$ .

With these definitions we can define powers (energy flows) associated with pathways:

$$P_p^f = A_p^{fT} V_p = (K_p^T A^f)^T V_p = A^{fT} K_p V_p = A^{fT} V = P^f \quad (17)$$

$$\text{similarly } P_p^r = A_p^{rT} V_p = (K_p^T A^r)^T V_p = A^{rT} K_p V_p = A^{rT} V = P^r \quad (18)$$

Thus the net forward pathway energy flow  $P_p^f$  equals the net forward reaction energy flow  $P^f$  and the net reverse pathway energy flow  $P_p^r$  equals the net reverse reaction energy flow  $P^r$ . Hence  $K_p$  can be considered as an energy transmitting transformer for both forward and backward pathway energies and is represented in Figure 2(b) by the symbol  $\mathcal{TF} : K_p$ .

Figure 2(c) can be obtained from Figure 2(b) by combining Equations (1) and (6) with Equation (12), and Equations (16) with Equations (4) to give:

$$\dot{X} = N_p V_p \quad A_p^f = N_p^{fT} \mu \quad A_p^r = N_p^{rT} \mu \quad (19)$$

$$\text{where } N_p = N K_p \quad N_p^f = N^f K_p \quad N_p^r = N^r K_p \quad (20)$$

Equation (20) defines the forward  $N_p^f$  and reverse  $N_p^r$  pathway stoichiometric matrices; using conditions (7) and (13), it follows that  $N_p^f$  and  $N_p^r$  have positive integer elements:

$$N_{p\ ij}^f \text{ is integer} \quad N_{p\ ij}^f \geq 0 \quad N_{p\ ij}^r \text{ is integer} \quad N_{p\ ij}^r \geq 0 \quad (21)$$

A property of  $N_p$  follows from combining Equations (20), (8) and (11); in particular,  $N_p$  may be rewritten as

$$N_p = (N^{cs} + N^{cd}) K_p = N^{cd} K_p = I^{cs} N K_p \quad (22)$$

Hence  $N_p$  has the property that the only non-zero rows correspond to the chemostats.

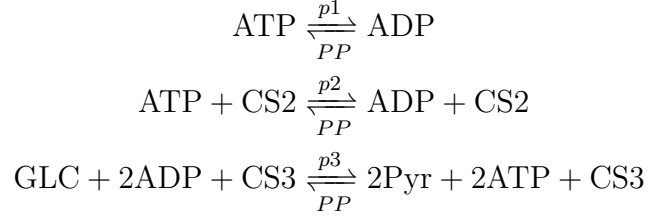
In the case of the example of Figure 1:

$$N_p = \begin{pmatrix} 0 & 0 & -1 \\ 0 & 0 & 2 \\ -1 & -1 & 2 \\ 1 & 1 & -2 \\ 0 & 0 & 0 \\ 0 & 0 & 0 \\ 0 & 0 & 0 \\ 0 & 0 & 0 \\ 0 & 0 & 0 \\ 0 & 0 & 0 \end{pmatrix} \quad N_p^f = \begin{pmatrix} 0 & 0 & 1 \\ 0 & 0 & 0 \\ 1 & 1 & 2 \\ 0 & 0 & 4 \\ 0 & 0 & 0 \\ 0 & 0 & 1 \\ 0 & 1 & 1 \\ 0 & 0 & 2 \\ 0 & 1 & 0 \\ 0 & 0 & 0 \end{pmatrix} \quad N_p^r = \begin{pmatrix} 0 & 0 & 0 \\ 0 & 0 & 2 \\ 0 & 0 & 4 \\ 1 & 1 & 2 \\ 0 & 0 & 0 \\ 0 & 0 & 1 \\ 0 & 1 & 1 \\ 0 & 0 & 2 \\ 0 & 1 & 0 \\ 0 & 0 & 0 \end{pmatrix} \quad (23)$$

Using Equation (19) and  $N_p$  from Equation (23), the affinity associated with each of the three pathways is, as expected:

$$A_{p1} = A_{p2} = \mu_{ATP} - \mu_{ADP} \quad A_{p3} = (\mu_{GLC} + 2\mu_{ADP}) - (2\mu_{Pyr} + 2\mu_{ATP}) \quad (24)$$

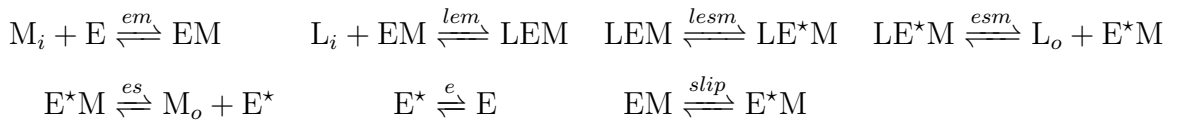
Because conditions (21) agree with conditions (7),  $N_p^f$  and  $N_p^r$  could correspond to the forward and reverse stoichiometric matrices of the following three reactions:



where  $\text{CS2} = \text{F6P} + \text{F2P}$  and  $\text{CS3} = 2\text{ATP} + 2\text{ADP} + \text{G6P} + \text{F6P} + 2\text{TP}$ . However, some care must be taken in this interpretation. Firstly, the kinetics are not mass-action even if the original equations correspond to mass-action kinetics. Secondly, and unlike conventional reactions, these three reactions are not independent; the consequences of this fact are discussed in §5. Nevertheless, such a pathway decomposition provides insight into the energy flows in a reaction network. This is illustrated using a generic example of Hill [14] in § 5 and using a specific example, the sodium-glucose transport protein of Eskandari et al. [33], in § 6.

## 5 Example: Free Energy Transduction and Biomolecular Cycles

In his classic monograph, “Free energy transduction and biomolecular cycle kinetics” Hill [14] discusses how the difference between the concentration of a species  $M_o$  outside a membrane and the concentration of the same species  $M_i$  inside the membrane can be used to transport another species  $L_i$  inside the membrane to outside the membrane  $L_o$  via a large protein molecule with two conformations  $E$  and  $E^*$  the former allowing successive binding to  $M_i$  and  $L_i$  and the latter to  $M_o$  and  $L_o$ . This biomolecular cycle is represented by the diagram of Figure 3(a) which corresponds to that of Hill [14, Figure 1.2(a)]. There are seven reactions



where the last reaction is the so-called *slippage*<sup>5</sup> term in which the enzyme changes conformation without transporting species L. The original Hill diagram does not name the seven reactions, they are named here to provide a link to the bond graph which explicitly names reactions.

The corresponding bond graph appears in Figure 3(b) where  $E^*$  is replaced by  $E_s$  for syntactical reasons. The bond graph clearly shows the cyclic structure of the chemical reactions and is geometrically similar to the diagram of Figure 3(a). As discussed by Hill [14], the four species  $M_o$ ,  $M_i$ ,  $L_o$  and  $L_i$ , are assumed to have constant concentration: therefore they are modelled by four chemostats.

<sup>5</sup>The term “slippage” was used in this context by Terrell L Hill in his seminal book [14]. An ideal cycle would have no slippage and the link from EM to  $E^*M$  would not exist in Figure 3(a).

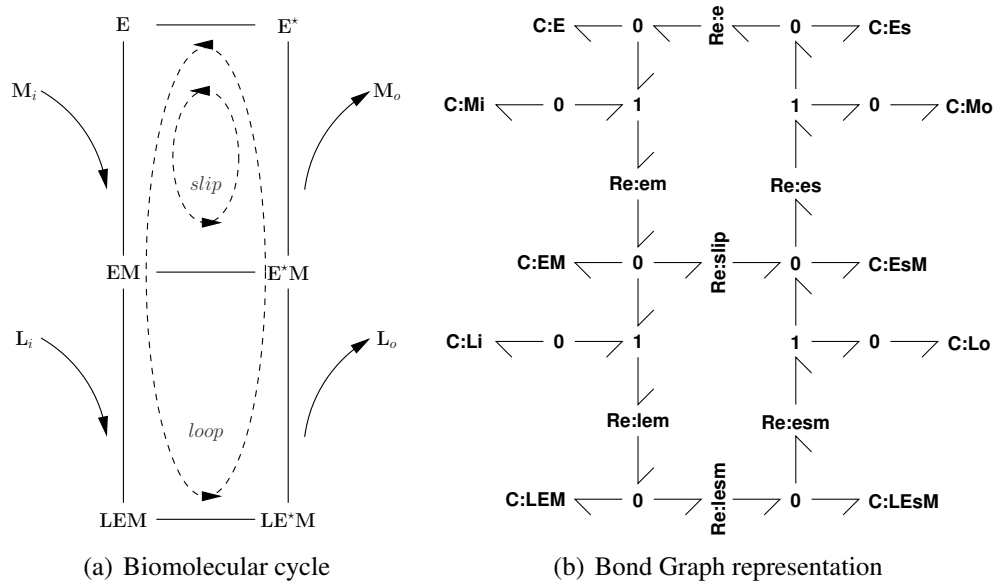
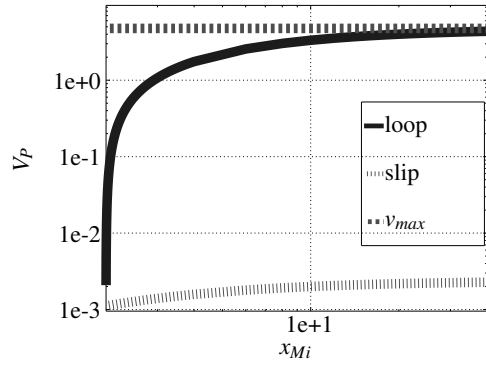
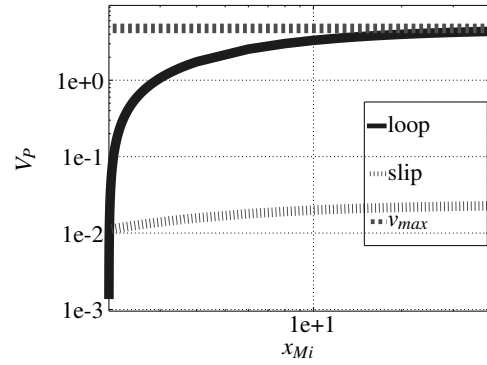


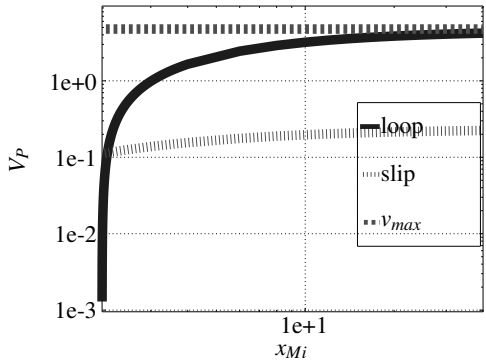
Figure 3: Free energy transduction and biomolecular cycles: model. (a) As discussed in the text, this is a generic model of a transmembrane transporter due to Hill [14] and based on the conformations of the protein  $E$  which uses the chemical gradient of  $M$  to pump  $L$  across the membrane against an adverse gradient. An ideal cycle would have no “slippage”: the link from  $EM$  to  $E^*M$  would not exist. As discussed in the text, two pathways: *loop* and *slip* have been marked. (b) The bond graph is geometrically the same as (a) but gives a precise description. ( $Es$  is used in place of  $E^*$  for syntactical reasons).



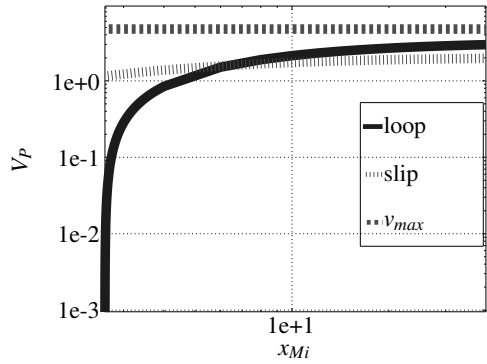
(a)  $\kappa_{slip} = 10^{-3}$



(b)  $\kappa_{slip} = 10^{-2}$



(c)  $\kappa_{slip} = 10^{-1}$



(d)  $\kappa_{slip} = 1$

Figure 4: Free energy transduction and biomolecular cycles: positive flow regime. (a) The flow in the two pathways labelled *loop* and *slip* in Figure 3(a) are shown together with the maximum flow  $v_{max}$  for slippage coefficient  $\kappa_{slip} = 10^{-3}$ . (b) – (d) show the same information for three further values of the slippage coefficient  $\kappa_{slip}$ .

The states  $X$ , stoichiometric matrix  $N$  and reaction flows  $V$  of this system are:

$$X = \begin{pmatrix} x_{L_i} \\ x_{L_o} \\ x_{M_i} \\ x_{M_o} \\ x_E \\ x_{EM} \\ x_{LEM} \\ x_{E^*} \\ x_{E^*M} \\ x_{LE^*M} \end{pmatrix}, \quad N = \begin{pmatrix} 0 & -1 & 0 & 0 & 0 & 0 & 0 \\ 0 & 0 & 0 & 1 & 0 & 0 & 0 \\ -1 & 0 & 0 & 0 & 0 & 0 & 0 \\ 0 & 0 & 0 & 0 & 1 & 0 & 0 \\ -1 & 0 & 0 & 0 & 0 & 1 & 0 \\ 1 & -1 & 0 & 0 & 0 & 0 & -1 \\ 0 & 1 & -1 & 0 & 0 & 0 & 0 \\ 0 & 0 & 0 & 0 & 1 & -1 & 0 \\ 0 & 0 & 0 & 1 & -1 & 0 & 1 \\ 0 & 0 & 1 & -1 & 0 & 0 & 0 \end{pmatrix}, \quad V = \begin{pmatrix} v_{em} \\ v_{lem} \\ v_{lesm} \\ v_{esm} \\ v_{es} \\ v_e \\ v_{slip} \end{pmatrix} \quad (25)$$

The matrix  $N^{cd}$  is the same as  $N$  but with the first four rows (corresponding to the four chemostats) deleted. The rank of  $N^{cd}$  is  $r = 5$  corresponding to the four chemostats and the conserved moiety of the remaining states; thus the null space has dimension  $n_V - r = 2$ .

As discussed in §4, two positive pathways were identified both by bond graph pathway analysis and using metatool<sup>6</sup>. The corresponding PPM  $K_p$  is:

$$K_p^T = \begin{pmatrix} 1 & 1 & 1 & 1 & 1 & 1 & 0 \\ 1 & 0 & 0 & 0 & 1 & 1 & 1 \end{pmatrix} \quad (26)$$

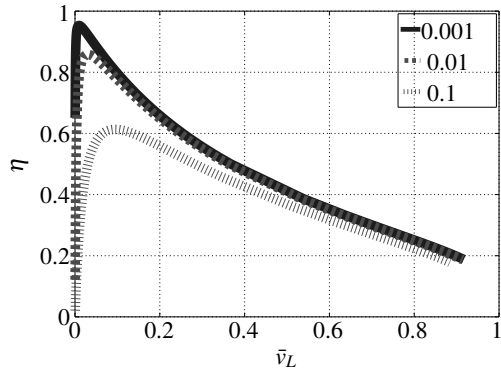
Apart from the ordering of the two columns, the PPM for this system is unique. These two columns correspond to the path involving the six reactions: {e em lem es esm lesm} and the upper loop involving the four reactions: {e em es slip}. These are the only positive pathways for this system. For convenience, the first (outer) pathway will be named *loop* and the second pathway (involving the “slip” reaction) will be named *slip*; this nomenclature is indicated in Figure 3(a).

For the purposes of illustration the thermodynamic constants of the ten species are taken to be unity, the total amount of E, EM, LEM, E\*, E\*M and LE\*M is taken as  $E_{tot} = 10$ , the amount of  $M_o$  and  $L_i$  is taken as unity, the amount of  $L_o$  as two and  $M_i$  is variable. The rate constant of the slippage reaction is varied in the sequel, and that of the other reactions is 10.

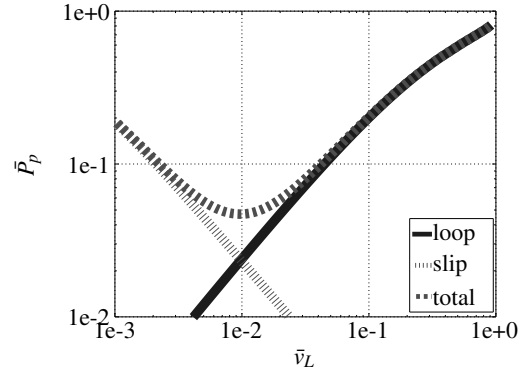
The system was simulated with a slow change of the amount of  $M_i$  from 2 to 100 such that the system was effectively in a steady state for each value of the amount of  $M_i$ ; these values were then refined using a steady-state finder. The conserved moiety was automatically accounted for using the method of Gawthrop and Crampin [29, §3(c)]. The results were checked using explicit expressions for the steady state values using the software of Qi et al. [37] which is based on the method of King & Altman. The system equations are given in the Supplementary Material.

Figure 4 shows the two pathway flows  $v_1^P$  and  $v_2^P$  against the amount  $x_{M_i}$  of  $M_i$  for four values of  $\kappa_{slip}$ . As derived in the Supplementary Material, the maximum flow when the  $\kappa_{slip} = 0$  is given by  $v_{max} = \frac{100}{21} = 4.76$  and this value is also plotted on each graph.

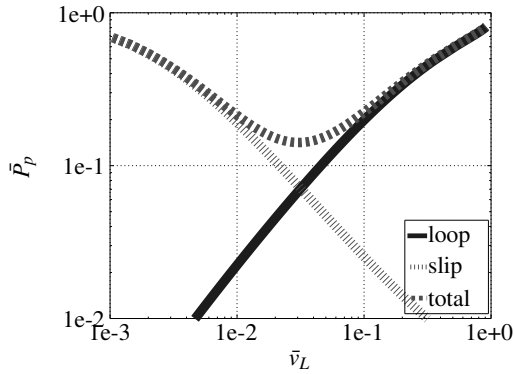
<sup>6</sup>The Octave [36] version of metatool from <http://penguin.biologie.uni-jena.de/bioinformatik/networks/metatool/metatool5.0/metatool5.0.html> was used.



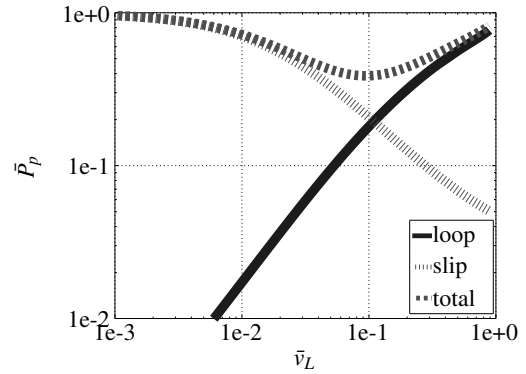
(a) Efficiency  $\eta$  for different  $\kappa_{slip}$



(b) Normalised dissipation  $\bar{P}_p$ :  $\kappa_{slip} = 10^{-3}$

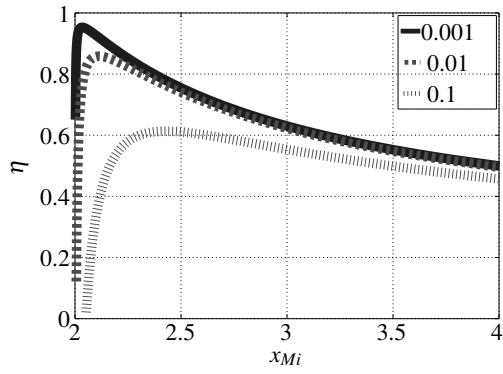


(c) Normalised dissipation  $\bar{P}_p$ :  $\kappa_{slip} = 10^{-2}$

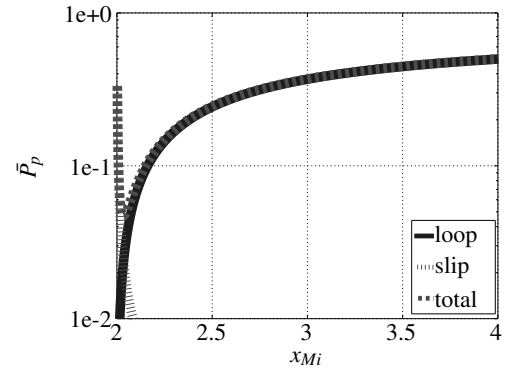


(d) Normalised dissipation  $\bar{P}_p$ :  $\kappa_{slip} = 10^{-1}$

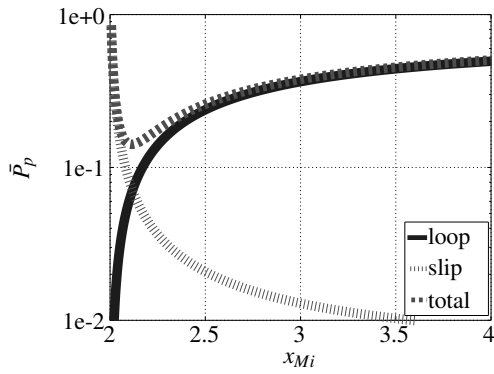
Figure 5: Free energy transduction and biomolecular cycles: Energy-based analysis. (a) The free energy transduction efficiency  $\eta$  is plotted against normalised flow  $\bar{v}_L$  of  $L$  for the three values of the slippage coefficient  $\kappa_{slip}$  used in b) – (d). (b) – (d) The normalised pathway free energy dissipation  $\bar{P}_p$  is plotted against normalised flow  $\bar{v}_L$  of  $L$  for the two pathways *loop* and *slip* marked on Figure 3(a) together with the total normalised free energy dissipation.



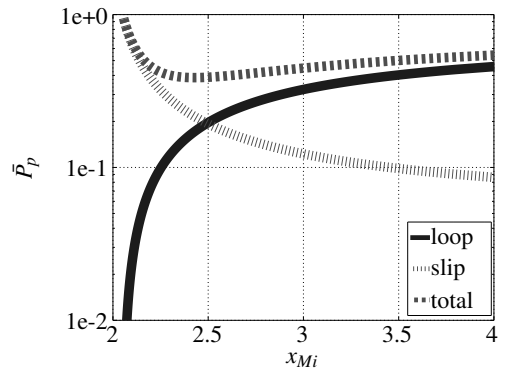
(a) Efficiency  $\eta$  for different  $\kappa_{slip}$



(b) Normalised dissipation  $\bar{P}_p$ :  $\kappa_{slip} = 10^{-3}$



(c) Normalised dissipation  $\bar{P}_p$ :  $\kappa_{slip} = 10^{-2}$



(d) Normalised dissipation  $\bar{P}_p$ :  $\kappa_{slip} = 10^{-1}$

Figure 6: Free energy transduction and biomolecular cycles: Energy-based analysis. Figure 5 is replotted with  $x_{Mi}$  replacing  $\bar{V}_L$



The purpose of this cycle is to use the excess of  $M$  to pump  $L$  against the concentration gradient. In addition to viewing the cycle as a mass transport system, it may also be viewed as a system for transducing free energy from  $M$  to  $L$ . From this point of view, it is interesting to investigate the (steady-state) *efficiency*  $\eta$  of the energy transduction [14, §1.4], which we define as:

$$\eta = \frac{P_L}{P_M} \quad \text{where } P_L = (\mu_{Lo} - \mu_{Li}) v_L \quad \text{and } P_M = (\mu_{Mi} - \mu_{Mo}) v_M \quad (27)$$

The simulated  $\eta$  is plotted against normalised flow  $\bar{v}_L = \frac{v_{Lo}}{v_{max}}$  in Figure 5(a) for the four values of  $\kappa_{slip}$  and reveals three features:

1. with negligible slip, the maximum efficiency occurs at low flow rates.
2. the efficiency decreases as  $\kappa_{slip}$  increases
3. the flow rate corresponding to maximum efficiency increases with  $\kappa_{slip}$ .

To further investigate the source of the inefficiency, the pathway dissipation  $P_p$  was computed and normalised to give  $\bar{P}_p = \frac{P_p}{P_M}$ . This is plotted for each pathway, together with the total normalised dissipation, against the normalised flow  $\bar{v}_L$  of L in Figures 5(b) – 5(d) for three values of  $\kappa_{slip}$ . As can be seen, the main loop pathway dissipation *increases* with flow of L with all of the free energy associated with M dissipated at the maximum flow rate. In contrast, the slippage pathway dissipation *decreases* with flow of L with all of the free energy associated with M dissipated at zero flow rate. The combined normalised dissipation thus has a minimum (i.e. energy transduction is most efficient) at an intermediate flow rate dependant on  $\kappa_{slip}$ .

Figure 6 is similar to Figure 5 except that the efficiency  $\eta$  and normalised energy flows  $\bar{P}_p$  are plotted against  $M_i$  in the positive flow regime. The minima occur at values of  $M_i$  towards the lower end of the positive flow regime. This reflects the fact that, as shown in Figure 4, large changes in flow  $v_P$  correspond to small changes in concentration  $x_{Mi}$  towards the lower end of the positive flow regime; for larger values of  $x_{Mi}$ , the effect of changes in  $x_{Mi}$  on  $v_P$  is smaller.

As mentioned in § 4, the reactions corresponding to the two pathways of this example are not independent. To examine the consequences of this interaction, Figure 7 focuses on the system behaviour in the crossover region where the two pathway flows have opposite directions. Figure 7(a) shows the two mass flows which have opposite sign in the crossover region  $0.42 < M_i < 2.62$  delineated by the two vertical lines. Within this region, Figure 7(b) shows that the individual pathway energy dissipations may be negative; of course, as indicated in Figure 7(b), the total dissipation remains positive. This behaviour is a consequence of the intersection of the two pathways leading to a non-diagonal  $\mathcal{PW}$  (Figure 2). Furthermore, the sum of the two pathway flows, corresponding to the flow of  $M_i$  and  $M_o$ , also changes sign thus causing the associated energy flow  $P_M$  (27) to also change sign. Thus normalising the pathway energy transduction in the crossover region using Equation (27) is not helpful. However, the normal operating region of such a biomolecular cycle is outside the crossover region and hence this situation does not normally arise.

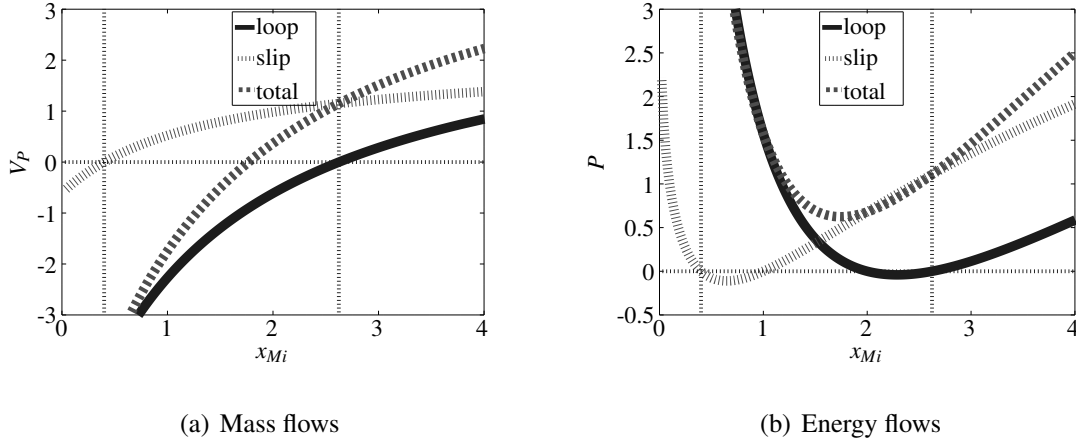


Figure 7: Mass and Energy flows in the crossover region. For sufficiently small  $M_i$ , the cycle no longer acts as a transporter as the flows in the two pathways labelled *loop* and *slip* in Figure 3(a) become negative. This figure examines the crossover regime (delineated by the two vertical lines) where one pathway flow is positive and the other negative – with a large value ( $\kappa_{slip} = 1$ ) of slippage to exaggerate the effect. Notice the negative pathway dissipations when the sign of the pathway flows is different – this is due to the intersection of the two pathways leading to a non-diagonal  $\mathcal{PW}$ .

## 6 Example: The Sodium-Glucose Transport Protein 1 (SGLT1)

The Sodium-Glucose Transport Protein 1 (SGLT1) (also known as the  $\text{Na}^+$ /glucose transporter) was studied experimentally by Parent et al. [38] and explained by a biophysical model [39]; further experiments and modelling were conducted by Chen et al. [40]. Eskandari et al. [33] examined the kinetics of the reverse mode using similar experiments and analysis to Parent et al. [38, 39] but with reverse transport and currents. This example looks at a bond graph based model of SGLT1 based on the model of Eskandari et al. [33]. For simplicity, it is assumed that the membrane potential is zero and thus there are no electrogenic effects.

The model of Eskandari et al. [33, Figure 6B], given in diagrammatic form in Figure 8(a) is based on the six-state biomolecular cycle of Figure 2 of Parent et al. [39]. When operating normally, sugar is transported from the outside to the inside of the membrane driven against a possibly adverse gradient by the concentration gradient of  $\text{Na}^+$ . The diagram of Figure 8(a) is similar to the Hill model of Figure 3(a). Apart from the renaming of components, and the reversal of inside and outside, the major difference is that the single driving molecule  $M_i$  and  $M_o$  replaced by *two* driving molecules  $2\text{Na}_o^+$  and  $2\text{Na}_i^+$ . This change is reflected in the bond graph of 8(b) by the double bonds. This also means that the stoichiometric matrix  $N$  is the same as that of Equation (25) except that the rows corresponding to  $\text{Na}_o^+$  and  $\text{Na}_i^+$  are multiplied by 2. However, as  $\text{Na}_o^+$  and  $\text{Na}_i^+$  are chemostats, this change does not affect the PPM  $K_p$  which is still given by (26). The actual matrices are given in the Supplementary Material. The seven sets of reaction kinetic parameters are given in Figure 6B Eskandari et al. [33] and listed in the first two

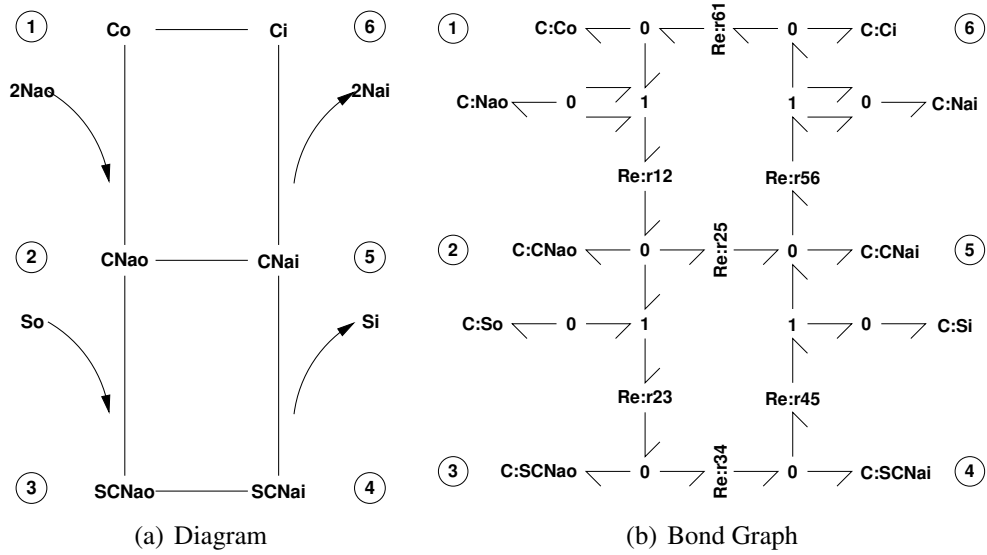


Figure 8: The Sodium-Glucose Transport Protein 1 (SGLT1). (a) Diagram with the six states marked. (b) The corresponding bond graph.

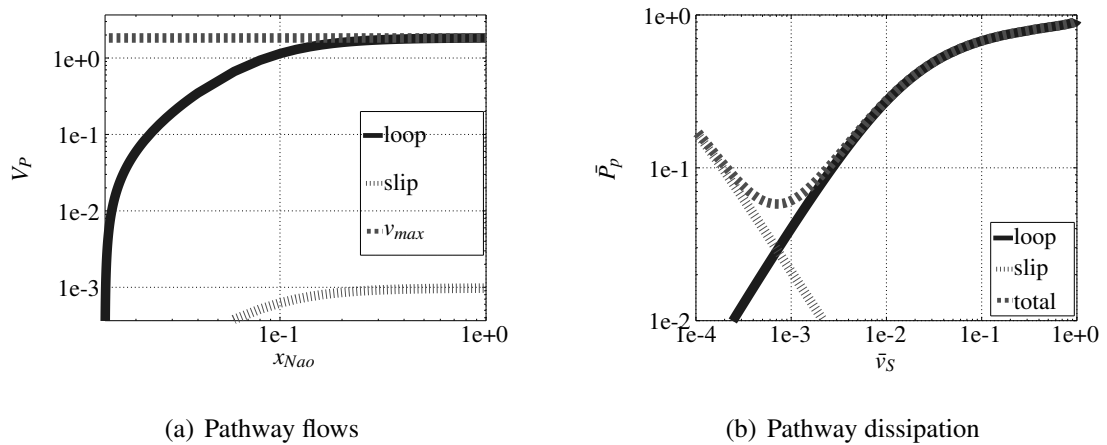


Figure 9: The Sodium-Glucose Transport Protein 1 (SGLT1). (a) Simulated flows (normalised) in the two pathways labelled *loop* and *slip* in Figure 3(a). (b) The normalised pathway dissipations as a function of normalised flows.

columns of Table 1 of the Supplementary Material and the third column gives the corresponding equilibrium constants. The vector of seven equilibrium constants  $K^{eq}$  is converted into the vector of ten thermodynamic constants  $K$  of Table 2 of the Supplementary Material using the formula of Gawthrop et al. [30]:

$$K^{eq} = \mathbf{Exp} \left( -N^T \mathbf{Ln} K \right) \quad (28)$$

where  $N$  is the  $10 \times 7$  stoichiometric matrix. The corresponding rate constants  $\kappa$  are then computed as discussed by Gawthrop et al. [30] and listed in the final column of Table 1 of the Supplementary Material. The system was simulated as described in § 5 and the system equations are given in the Supplementary Material.

As in Figure 4, Figure 9(a) shows the two pathway flows and, as in Figure 5, Figure 9(b) shows the corresponding pathway dissipation. As in § 5, but using parameters corresponding to experimental data, the combined normalised dissipation has a minimum (i.e. energy transduction is most efficient) at an intermediate flow rate.

## 7 Conclusion

It has been shown that standard methods of mass-flow pathway analysis can be extended to energy-flow pathway analysis making use of the bond graph method arising from engineering science. The method has been applied to a glycolysis example of Heinrich and Schuster [5, Figure 3.4] and the biomolecular cycle of Hill [14, Figure 1.2(a)] to enable comparison with standard approaches.

The analysis of the biomolecular transporter cycle was shown to apply to a model of the Sodium-Glucose Transport Protein 1 (SGLT1) based on the experimentally-determined parameters of Eskandari et al. [33, Figure 6B]. Intriguingly, it was found that the rate of energy dissipation has a minimum value at a particular normalised flow rate which in turn corresponds to a particular driving concentration. This minimum is due to the interaction of a number of factors including the system parameters, the presence of two interacting pathways and the concentration of  $\text{Na}^+$  (or  $M$  in the case of § 5) needed to generate the transporter flow. It would be interesting to compare this theoretical flow rate to that found in nature.

The bond graph approach can be used to decompose complex systems into computational modules [30, 31]. Combining such modularity with energy-based pathway analysis approach of this paper would provide an approach to analysing and understanding energy flows in complex biomolecular systems for example those within the Physiome Project [41]. This is the subject of current research.

Although this paper is restricted to flows of chemical energy, the bond graph approach enables models to be built across multiple energy domains including chemo-electrical transduction [42, 43]. Hence the pathway approach can be equally well applied to systems with electrogenic features such as excitable membranes [44] and the mitochondrial electron transport chain [45].

The effective use of energy is an important determinant of evolution [13, 46, 47, 17]. Therefore the energy-based pathway analysis of this paper is potentially relevant to investigating why living systems have evolved as they have. For example, do real SGLT1 transporters operate near the point of minimal energy dissipation?

The supply of energy is essential to life and disruption of energy supply has been implicated in many diseases such as cardiac failure [48, 49], Parkinson's disease [50–54] and cancer [55–57]. Therefore it seems natural to apply the energy-based methods of this paper to investigate such systems. In particular, mitochondria are important for energy transduction in living systems and mitochondrial dysfunction is hypothesised to be the source of ageing [58, Chapter 14], cancer [59, 60] and other diseases [61]. Mathematical models of mitochondria exist already [62–65] and it is hoped that the energy-based pathway analysis of this paper will shed further light on the function and dysfunction of mitochondria. This is the subject of current research.

## Data accessibility

A virtual reference environment [66] is available for this paper at <http://dx.doi.org/10.5281/zenodo.165180>. The simulation parameters are listed in the Appendix.

## Competing interests

The authors have no competing interests.

## Authors' contribution

All authors contributed to drafting and revising the paper, and they affirm that they have approved the final version of the manuscript.

## Acknowledgements

Peter Gawthrop would like to thank the Melbourne School of Engineering for its support via a Professorial Fellowship. Both authors thank Dr Ivo Siekmann for discussions relating to conic spaces and Dr Daniel Hurley for help with the virtual reference environment. We would also like to thank the reviewers for their suggestions for improving the paper and Peter Hunter for pointing out some errors in the draft ms.

## Funding statement

This research was in part conducted and funded by the Australian Research Council Centre of Excellence in Convergent Bio-Nano Science and Technology (project number CE140100036).

## References

- [1] Purvesh Khatri, Marina Sirota, and Atul J. Butte. Ten years of pathway analysis: Current approaches and outstanding challenges. *PLoS Comput Biol*, 8(2):e1002375, 02 2012. doi:10.1371/journal.pcbi.1002375.

- [2] Conner I. Sandefur, Maya Mincheva, and Santiago Schnell. Network representations and methods for the analysis of chemical and biochemical pathways. *Mol. BioSyst.*, 9:2189–2200, 2013. doi:10.1039/C3MB70052F.
- [3] Jason A. Papin, Joerg Stelling, Nathan D. Price, Steffen Klamt, Stefan Schuster, and Bernhard O. Palsson. Comparison of network-based pathway analysis methods. *Trends in Biotechnology*, 22(8):400 – 405, 2004. ISSN 0167-7799. doi:10.1016/j.tibtech.2004.06.010.
- [4] Bruce L. Clarke. Stoichiometric network analysis. *Cell Biophysics*, 12(1):237–253, 1988. ISSN 1559-0283. doi:10.1007/BF02918360.
- [5] Reinhart Heinrich and Stefan Schuster. *The regulation of cellular systems*. Chapman & Hall New York, 1996.
- [6] Bernhard Palsson. *Systems biology: properties of reconstructed networks*. Cambridge University Press, 2006. ISBN 0521859034.
- [7] Bernhard Palsson. *Systems Biology: Simulation of Dynamic Network States*. Cambridge University Press, 2011.
- [8] Edda Klipp, Wolfram Liebermeister, Christoph Wierling, Axel Kowald, Hans Lehrach, and Ralf Herwig. *Systems biology*. Wiley-Blackwell, 2011.
- [9] Stefan Schuster and Claus Hilgetag. On elementary flux modes in biochemical reaction systems at steady state. *Journal of Biological Systems*, 2(02):165–182, 1994.
- [10] T Pfeiffer, I Sanchez-Valdenebro, J C Nuno, F Montero, and S Schuster. Meta-tool: for studying metabolic networks. *Bioinformatics*, 15(3):251–257, 1999. doi:10.1093/bioinformatics/15.3.251.
- [11] Christophe H. Schilling, David Letscher, and Bernhard Palsson. Theory for the systemic definition of metabolic pathways and their use in interpreting metabolic function from a pathway-oriented perspective. *Journal of Theoretical Biology*, 203(3):229 – 248, 2000. ISSN 0022-5193. doi:10.1006/jtbi.2000.1073.
- [12] S. Schuster, C. Hilgetag, J.H. Woods, and D.A. Fell. Reaction routes in biochemical reaction systems: Algebraic properties, validated calculation procedure and example from nucleotide metabolism. *Journal of Mathematical Biology*, 45(2):153–181, 2002. ISSN 0303-6812. doi:10.1007/s002850200143.
- [13] Alfred J. Lotka. Contribution to the energetics of evolution. *Proc Natl Acad Sci U S A*, 8(6):147–151, Jun 1922. ISSN 0027-8424.
- [14] Terrell L Hill. *Free energy transduction and biochemical cycle kinetics*. Springer-Verlag, New York, 1989.

- [15] Hong Qian, Daniel A. Beard, and Shou-dan Liang. Stoichiometric network theory for nonequilibrium biochemical systems. *European Journal of Biochemistry*, 270(3):415–421, 2003. ISSN 1432-1033. doi:10.1046/j.1432-1033.2003.03357.x.
- [16] Daniel A Beard and Hong Qian. *Chemical biophysics: quantitative analysis of cellular systems*. Cambridge University Press, 2010.
- [17] William F. Martin, Filipa L. Sousa, and Nick Lane. Energy at life’s origin. *Science*, 344(6188):1092–1093, 2014. ISSN 0036-8075. doi:10.1126/science.1251653.
- [18] H. M. Paynter. *Analysis and design of engineering systems*. MIT Press, Cambridge, Mass., 1961.
- [19] Dean C Karnopp, Donald L Margolis, and Ronald C Rosenberg. *System Dynamics: Modeling, Simulation, and Control of Mechatronic Systems*. John Wiley & Sons, 5th edition, 2012. ISBN 978-0470889084.
- [20] F. E. Cellier. *Continuous system modelling*. Springer-Verlag, 1991.
- [21] P. J. Gawthrop and L. P. S. Smith. *Metamodelling: Bond Graphs and Dynamic Systems*. Prentice Hall, Hemel Hempstead, Herts, England., 1996. ISBN 0-13-489824-9.
- [22] Peter J Gawthrop and Geraint P Bevan. Bond-graph modeling: A tutorial introduction for control engineers. *IEEE Control Systems Magazine*, 27(2):24–45, April 2007. doi:10.1109/MCS.2007.338279.
- [23] Wolfgang Borutzky. *Bond Graph Modelling of Engineering Systems: Theory, Applications and Software Support*. Springer, 2011. ISBN 9781441993670.
- [24] Wolfgang Borutzky, editor. *Bond Graphs for Modelling, Control and Fault Diagnosis of Engineering Systems*. Springer New York, 2017. doi:10.1007/978-3-319-47434-2. In press.
- [25] J. Greifeneder and F.E. Cellier. Modeling chemical reactions using bond graphs. In *Proceedings ICBGM12, 10th SCS Intl. Conf. on Bond Graph Modeling and Simulation*, pages 110–121, Genoa, Italy, 2012.
- [26] Vanessa Diaz-Zuccarini and Cesar Pichardo-Almarza. On the formalization of multi-scale and multi-science processes for integrative biology. *Interface Focus*, 1(3):426–437, 2011. doi:10.1098/rsfs.2010.0038.
- [27] George Oster, Alan Perelson, and Aharon Katchalsky. Network thermodynamics. *Nature*, 234:393–399, December 1971. doi:10.1038/234393a0.
- [28] George F. Oster, Alan S. Perelson, and Aharon Katchalsky. Network thermodynamics: dynamic modelling of biophysical systems. *Quarterly Reviews of Biophysics*, 6(01):1–134, 1973. doi:10.1017/S0033583500000081.

- [29] Peter J. Gawthrop and Edmund J. Crampin. Energy-based analysis of biochemical cycles using bond graphs. *Proceedings of the Royal Society A: Mathematical, Physical and Engineering Science*, 470(2171):1–25, 2014. doi:10.1098/rspa.2014.0459. Available at arXiv:1406.2447.
- [30] Peter J. Gawthrop, Joseph Cursons, and Edmund J. Crampin. Hierarchical bond graph modelling of biochemical networks. *Proceedings of the Royal Society A: Mathematical, Physical and Engineering Sciences*, 471(2184):1–23, 2015. ISSN 1364-5021. doi:10.1098/rspa.2015.0642. Available at arXiv:1503.01814.
- [31] P. J. Gawthrop and E. J. Crampin. Modular bond-graph modelling and analysis of biomolecular systems. *IET Systems Biology*, 10(5):187–201, October 2016. ISSN 1751-8849. doi:10.1049/iet-syb.2015.0083. Available at arXiv:1511.06482.
- [32] Peter J. Gawthrop. Bond-graph modelling and causal analysis of biomolecular systems. In Wolfgang Borutzky, editor, *Bond Graphs for Modelling, Control and Fault Diagnosis of Engineering Systems*, pages 587–623. Springer International Publishing, Berlin, 2017. ISBN 978-3-319-47434-2. doi:10.1007/978-3-319-47434-2\_16.
- [33] S. Eskandari, E. M. Wright, and D. D. F. Loo. Kinetics of the Reverse Mode of the Na<sup>+</sup>/Glucose Cotransporter. *J Membr Biol*, 204(1):23–32, Mar 2005. ISSN 0022-2631. doi:10.1007/s00232-005-0743-x. 16007500[pmid].
- [34] Matteo Polettini and Massimiliano Esposito. Irreversible thermodynamics of open chemical networks. I. Emergent cycles and broken conservation laws. *The Journal of Chemical Physics*, 141(2):024117, 2014. doi:10.1063/1.4886396.
- [35] Martin Aigner and Günter M Ziegler. *Proofs from the Book*. Springer, Berlin, 5th edition, 2014.
- [36] John W. Eaton, David Bateman, Søren Hauberg, and Rik Wehbring. *GNU Octave version 4.0.0 manual: a high-level interactive language for numerical computations*, 2015. URL <http://www.gnu.org/software/octave/doc/interpreter>.
- [37] Feng Qi, Ranjan K. Dash, Yu Han, and Daniel A. Beard. Generating rate equations for complex enzyme systems by a computer-assisted systematic method. *BMC Bioinformatics*, 10(1):1–9, 2009. ISSN 1471-2105. doi:10.1186/1471-2105-10-238.
- [38] Lucie Parent, Stéphane Supplisson, Donald D. F. Loo, and Ernest M. Wright. Electrogenic properties of the cloned Na<sup>+</sup>/glucose cotransporter: I. voltage-clamp studies. *The Journal of Membrane Biology*, 125(1):49–62, 1992. ISSN 1432-1424. doi:10.1007/BF00235797.
- [39] Lucie Parent, Stéphane Supplisson, Donald D. F. Loo, and Ernest M. Wright. Electrogenic properties of the cloned Na<sup>+</sup>/glucose cotransporter: II. a transport model under nonrapid equilibrium conditions. *The Journal of Membrane Biology*, 125(1):63–79, 1992. ISSN 1432-1424. doi:10.1007/BF00235798.



- [40] Xing-Zhen Chen, Michael J Coady, Francis Jackson, Alfred Berteloot, and Jean-Yves Lapointe. Thermodynamic determination of the Na<sup>+</sup>: glucose coupling ratio for the human SGLT1 cotransporter. *Biophysical Journal*, 69(6):2405, 1995. doi:10.1016/S0006-3495(95)80110-4.
- [41] Peter Hunter. The virtual physiological human: The physiome project aims to develop reproducible, multiscale models for clinical practice. *IEEE Pulse*, 7(4):36–42, July 2016. ISSN 2154-2287. doi:10.1109/MPUL.2016.2563841.
- [42] Dean Karnopp. Bond graph models for electrochemical energy storage : electrical, chemical and thermal effects. *Journal of the Franklin Institute*, 327(6):983 – 992, 1990. ISSN 0016-0032. doi:10.1016/0016-0032(90)90073-R.
- [43] Peter J. Gawthrop, Ivo Siekmann, Tatiana Kameneva, Susmita Saha, Michael R. Ibbotson, and Edmund J. Crampin. The Energetic Cost of the Action Potential: Bond Graph Modelling of Electrochemical Energy Transduction in Excitable Membranes. Available at arXiv:1512.00956, 2015.
- [44] Bertil Hille. *Ion Channels of Excitable Membranes*. Sinauer Associates, Sunderland, MA, USA, 3rd edition, 2001. ISBN 978-0-87893-321-1.
- [45] David G Nicholls and Stuart Ferguson. *Bioenergetics 4*. Academic Press, Amsterdam, 2013.
- [46] Filipa L. Sousa, Thorsten Thiergart, Giddy Landan, Shijulal Nelson-Sathi, Inês A. C. Pereira, John F. Allen, Nick Lane, and William F. Martin. Early bioenergetic evolution. *Philosophical Transactions of the Royal Society of London B: Biological Sciences*, 368 (1622), 2013. ISSN 0962-8436. doi:10.1098/rstb.2013.0088.
- [47] Robert Pascal, Addy Pross, and John D. Sutherland. Towards an evolutionary theory of the origin of life based on kinetics and thermodynamics. *Open Biology*, 3(11), 2013. doi:10.1098/rsob.130156.
- [48] Stefan Neubauer. The failing heart – an engine out of fuel. *New England Journal of Medicine*, 356(11):1140–1151, 2007. doi:10.1056/NEJMra063052.
- [49] Kenneth Tran, Denis S. Loiselle, and Edmund J. Crampin. Regulation of cardiac cellular bioenergetics: mechanisms and consequences. *Physiological Reports*, 3(7):e12464, 2015. ISSN 2051-817X. doi:10.14814/phy2.12464.
- [50] M. Flint Beal. Does impairment of energy metabolism result in excitotoxic neuronal death in neurodegenerative illnesses? *Annals of Neurology*, 31(2):119–130, 1992. ISSN 1531-8249. doi:10.1002/ana.410310202.
- [51] Peter Wellstead and Mathieu Cloutier. An energy systems approach to Parkinson’s disease. *Wiley Interdisciplinary Reviews: Systems Biology and Medicine*, 3(1):1–6, 2011. ISSN 1939-005X. doi:10.1002/wsbm.107.

- [52] Zu-Hang Sheng and Qian Cai. Mitochondrial transport in neurons: impact on synaptic homeostasis and neurodegeneration. *Nat Rev Neurosci*, 13(2):77–93, Feb 2012. ISSN 1471-003X. doi:10.1038/nrn3156.
- [53] Peter Wellstead and Mathieu Cloutier, editors. *Systems Biology of Parkinson’s Disease*. Springer New York, 2012. ISBN 978-1-4614-3411-5. doi:10.1007/978-1-4614-3411-5.
- [54] Peter Wellstead. *A New Look at Disease: Parkinson’s through the eyes of an engineer*. Control Systems Principles, Stockport, UK, 2012. ISBN 978-0-9573864-0-2.
- [55] Alvaro Marin-Hernandez, Juan Carlos Gallardo-Perez, Sara Rodriguez-Enriquez, Rusely Encalada, Rafael Moreno-Sanchez, and Emma Saavedra. Modeling cancer glycolysis. *Biochimica et Biophysica Acta (BBA) - Bioenergetics*, 1807(6):755 – 767, 2011. ISSN 0005-2728. doi:10.1016/j.bbabi.2010.11.006. Bioenergetics of Cancer.
- [56] Alvaro Marin-Hernandez, Sayra. Lopez-Ramirez, JuanCarlos Gallardo-Perez, Sara Rodriguez-Enriquez, Rafael Moreno-Sanchez, and Emma Saavedra. Systems biology approaches to cancer energy metabolism. In Miguel A. Aon, Valdur Saks, and Uwe Schlatter, editors, *Systems Biology of Metabolic and Signaling Networks*, volume 16 of *Springer Series in Biophysics*, pages 213–239. Springer Berlin Heidelberg, 2014. ISBN 978-3-642-38504-9. doi:10.1007/978-3-642-38505-6\_9.
- [57] Ali Masoudi-Nejad and Yazdan Asgari. Metabolic cancer biology: structural-based analysis of cancer as a metabolic disease, new sights and opportunities for disease treatment. *Seminars in cancer biology*, 30:21–29, 2014.
- [58] Bruce Alberts, Alexander Johnson, Julian Lewis, David Morgan, Martin Raff, Keith Roberts, and Peter Walter., editors. *Molecular Biology of the Cell*. Garland Science, Abingdon, UK, sixth edition, 2015.
- [59] Vladimir Gogvadze, Sten Orrenius, and Boris Zhivotovsky. Mitochondria in cancer cells: what is so special about them? *Trends in Cell Biology*, 18(4):165 – 173, 2008. ISSN 0962-8924. doi:10.1016/j.tcb.2008.01.006.
- [60] Giancarlo Solaini, Gianluca Sgarbi, and Alessandra Baracca. Oxidative phosphorylation in cancer cells. *Biochimica et Biophysica Acta (BBA) - Bioenergetics*, 1807(6):534 – 542, 2011. ISSN 0005-2728. doi:10.1016/j.bbabi.2010.09.003. Bioenergetics of Cancer.
- [61] Jodi Nunnari and Anu Suomalainen. Mitochondria: In sickness and in health. *Cell*, 148(6): 1145 – 1159, 2012. ISSN 0092-8674. doi:10.1016/j.cell.2012.02.035.
- [62] Daniel A Beard. A biophysical model of the mitochondrial respiratory system and oxidative phosphorylation. *PLoS Comput Biol*, 1(4):e36, 09 2005. doi:10.1371/journal.pcbi.0010036.
- [63] Fan Wu, Feng Yang, Kalyan C. Vinnakota, and Daniel A. Beard. Computer modeling of mitochondrial tricarboxylic acid cycle, oxidative phosphorylation, metabolite transport,

- and electrophysiology. *Journal of Biological Chemistry*, 282(34):24525–24537, 2007. doi:10.1074/jbc.M701024200.
- [64] Sonia Cortassa and Miguel A. Aon. Dynamics of Mitochondrial Redox and Energy Networks: Insights from an Experimental-Computational Synergy. In Miguel A. Aon, Valdur Saks, and Uwe Schlattner, editors, *Systems Biology of Metabolic and Signaling Networks*, volume 16 of *Springer Series in Biophysics*, pages 115–144. Springer Berlin Heidelberg, 2014. ISBN 978-3-642-38504-9. doi:10.1007/978-3-642-38505-6\_5.
- [65] Jason N. Bazil, Daniel A. Beard, and Kalyan C. Vinnakota. Catalytic coupling of oxidative phosphorylation, ATP demand, and reactive oxygen species generation. *Biophysical Journal*, 110(4):962 – 971, 2016. ISSN 0006-3495. doi:10.1016/j.bpj.2015.09.036.
- [66] Daniel G. Hurley, David M. Budden, and Edmund J. Crampin. Virtual reference environments: a simple way to make research reproducible. *Briefings in Bioinformatics*, 2014. doi:10.1093/bib/bbu043.

## A A Short Introduction to Bond Graph Modelling

The purpose of this section is to provide the bond graph background necessary to understand the paper itself. More information is to be found in references [29–32].

Bond graphs unify the modelling of energy within and across multiple physical domains using the concepts of *effort* and *flow* variables whose product is *power*. Thus in the electrical domain the effort variable voltage  $V$  with units of V and flow variable current  $i$  with units of A have the product  $P = Vi$  with units of  $\text{J s}^{-1}$ . In the biomolecular domain, the effort variable is *chemical potential*  $\mu$  with units of  $\text{J/mol}$  and the flow variable is reaction flow rate  $v$  with units of  $\text{mol/sec}$ ;  $\mu v$  also has units of  $\text{J s}^{-1}$ .

The bond graph **C** component is a generic energy *storage* component corresponding to a *capacitor* in the electrical domain and the amount of a chemical species in the biomolecular domain. If  $q$  is the time integral of the flow variable, the electrical capacitor generates voltage  $V$  according to the *linear* relationship:  $V = q/C$  where  $C$  is the capacitance in Farads and  $q$  the charge in Coulombs. In contrast, the chemical species generates chemical potential  $\mu \text{J mol}^{-1}$  according to the *nonlinear* relationship:  $\mu = RT \ln Kx$  where  $R$  is the universal gas constant with units of  $\text{J mol}^{-1} \text{K}^{-1}$ ,  $T$  absolute temperature with units of K,  $x = q/q_0$  where  $q_0$  is the reference quantity and  $K$  a species-dependant constant which is dimensionless and depends on the reference quantity.

The bond graph **R** component is a generic energy *dissipation* component corresponding to a *resistor* in the electrical domain. In the linear case, it generates current  $i$  according to the *linear* relationship:  $i = \kappa \Delta V$  where  $\kappa$  is the conductance and  $\Delta V$  is the net voltage across the resistor. The **R** component corresponds a chemical *reaction* in the biomolecular domain. Assuming mass-action kinetics it generates molar flow  $v$  according to the *nonlinear* relationship:  $v = \kappa(\exp A^f/RT - \exp A^r/RT)$  where  $A^f$  (the *forward affinity*) and  $A^r$  (the *reverse affinity*) are

the net chemical potentials (with units of  $\text{J mol}^{-1}$ ) of the reactants and products of the reaction respectively;  $\kappa$  is the reaction *rate constant* with units of  $\text{mol s}^{-1}$ . Because this relationship treats the forward and reverse affinities differently, this reaction version of the **R** component is given a special symbol: **Re**.

Bond graphs represent the flow of energy between components by the bond symbol  $\rightarrow$  where the direction of the harpoon corresponds to the direction of positive energy flow; this is a sign convention. The bonds connect components via *junctions* which transmit, but do not store or dissipate energy. There are two junctions: the **0** junction where all impinging bonds have the same *effort* and the **1** junction where all impinging bonds have the same *flow*. The expression for the flows associated with the **0** junction, and the efforts associated with the **1** junction, are determined by the energy conservation requirement.

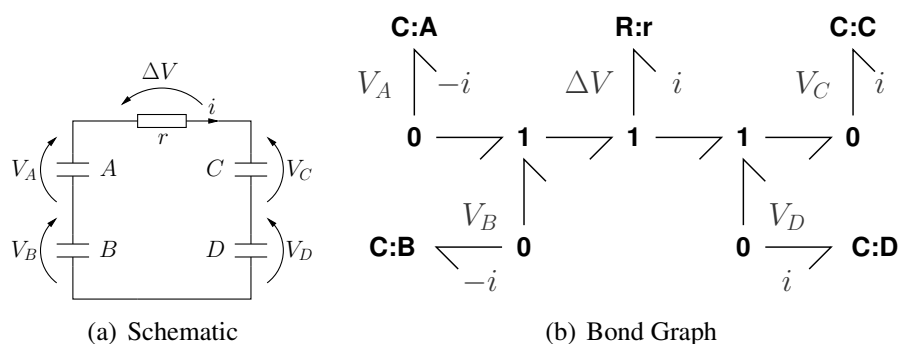


Figure 10: Modelling Electrical Systems. (a) Electrical schematic diagram. (b) Bond graph:  $\Delta V = (V_A + V_B) - (V_C + V_D)$ .

Figure 10 illustrates bond graph modelling in the electrical domain. The four capacitors and one resistor are connected as in the schematic diagram of Figure 10(a). In bond graph colon notation, the symbol before the colon indicates the component type and the symbol after the colon indicates the component name. Thus the bond graph of Figure 10(b) has four **C** components named A–D to represent the four capacitors and a single **R** component named r to represent the resistor. The two **0** junctions on the left reverse the sign of the flow associated with **C:A** and **C:B**. The two **0** junctions on the right are not necessary, but are convenient for connecting to other via bonds components to form a larger system. The left **1** junction corresponds to  $V^f = V_A + V_B$  and the right **1** junction corresponds to  $V^r = V_C + V_D$ ; the centre **1** junction corresponds to  $\Delta V = V^f - V^r = (V_A + V_B) - (V_C + V_D)$ . Given the constitutive relations for the **C** and **R** component, the dynamical equations describing the system can be automatically generated from the bond graph of Figure 10(b).

Figure 11 illustrates bond graph modelling in the chemical domain; the corresponding reaction is  $A + B \rightleftharpoons C + D$ . In a similar manner to the electrical system of Figure 10, the bond graph of Figure 11(b) has four **C** components named A–D to represent the four species and a single **Re** component named r to represent the reaction. The major difference is the use of the **Re** component to replace the **1** & **R** combination within the dotted box of Figure 10(b); as mentioned previously this is because the forward and reverse affinities are treated differently. In

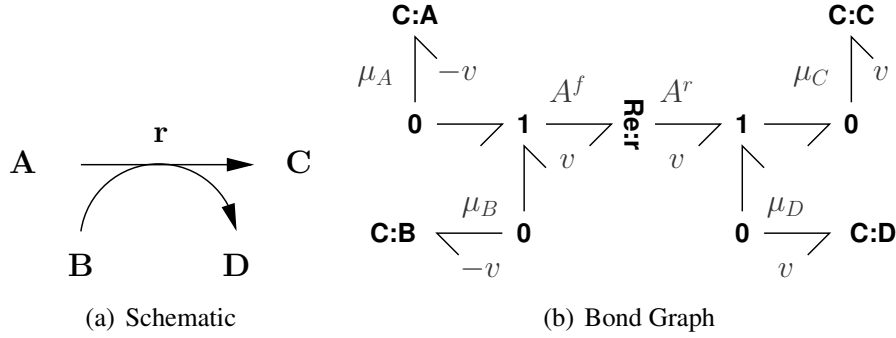


Figure 11: Modelling Biomolecular Systems:  $A + B \xrightleftharpoons{r} C + D$ . (a) Biomolecular schematic diagram. (b) Bond graph:  $A^f = \mu_A + \mu_B$ ,  $A^r = \mu_C + \mu_D$ .

particular, with reference to the example of Figure 11,  $A^f = \mu_A + \mu_B$ ,  $A^r = \mu_C + \mu_D$  which, with reference to Equation (4) corresponds to

$$N^f = (1 \quad 1 \quad 0 \quad 0n)^T \quad N^r = (0 \quad 0 \quad 1 \quad 1)^T$$

Using Equations (3) and (5), it follows that

$$\begin{aligned} A^f &= RT (\ln K_A x_A + \ln K_B x_B) = RT \ln K_A x_A K_B x_B \\ A^r &= RT (\ln K_C x_C + \ln K_D x_D) = RT \ln K_C x_C K_D x_D \\ \text{and } V &= \kappa_r \left( e^{\frac{A^f}{RT}} - e^{\frac{A^r}{RT}} \right) = \kappa_r (K_A x_A K_B x_B - K_C x_C K_D x_D) \end{aligned}$$

This is a form of the mass-action kinetics equation discussed in the textbooks [8]. In particular the equation can be rewritten as:

$$\begin{aligned} V &= k_f x_A x_B - k_r x_C x_D \\ \text{where } k_f &= \kappa K_A K_B \text{ and } k_r = \kappa K_D K_C \end{aligned}$$

As mentioned above, the  $K$  constants are dimensionless and thus  $k_f$  and  $k_r$  are dimensionless. The dimensionless *equilibrium constant*  $K_{eq}$  is defined as:

$$K_{eq} = \frac{k_f}{k_r}$$

As discussed by Gawthrop et al. [30],  $K_{eq}$  and  $K_A$ ,  $K_B$ ,  $K_C$  and  $K_D$  are related by the general formula (28).

In both the electrical and biomolecular systems there is only one flow: the current  $i$  in the electrical case and the molar flow  $v$  in the biomolecular case. This flow  $f$  is *out* of **C:A** and **C:B** and *into* **C:C** and **C:D**. Hence, in the biomolecular case,  $-\dot{x}_A = -\dot{x}_B = \dot{x}_C = \dot{x}_D = v$ . This implies that  $x_A + x_C = x_{AC}$ ,  $x_A + x_D = x_{AD}$  and  $x_B + x_C = x_{BC}$  where  $x_{AC}$ ,  $x_{AD}$  and  $x_{BC}$  are constant. Each of these three equations represents a *conserved moiety*: the total amount of

the charge or species involved remains constant. The choice of conserved moieties in a given situation is generally not unique; this is discussed further in § B.

Replacing A,B,C and D by GLC, G6P, ATP and ADP respectively and r by r4 in Figure 11 corresponds to the reaction to the left of the diagram in Figure 1. The apparently redundant **0** junctions in Figure 11 are used to provide connections between this particular reaction and the overall reaction network of Figure 1. The reaction diagram of Figure 1(a) has the entities ATP and ADP represented more than once. Although this enhances clarity by removing the need for intersecting lines on the diagram, it reduces clarity by having each entity appear in multiple locations. In contrast, the bond graph of Figure 1(b) represents ATP and ADP each by a single **C** component (**ATP** and **ADP** respectively) with appropriate connections to each of the reactions represented by **Re:r1** – **Re:r9**.

This idea of representing biomolecular reaction networks by **C** components (representing species) and **Re** components (representing reactions) connected by bonds ( $\rightarrow$ ) and **0** and **1** junctions is summarised and formalised in Figure 2(a). This representation is summarised in the caption to Figure 2 and is discussed in detail by Gawthrop and Crampin [29, 31].

Bond graphs provide one foundation for this paper, the other is the systems biology concept of *pathways* outlined in the next section.

## B A Short Introduction to Systems Biology

The purpose of this section is to provide the systems biology background necessary to understand the paper itself.

As discussed in the basic textbooks (for example that of Klipp et al. [8]), the *stoichiometric matrix*  $N$  is a fundamental construct in describing and understanding biomolecular systems. In particular, given  $n_X$  chemical species with molar amounts contained in the column vector  $X$  and  $n_V$  reactions with molar flow rates contained in the column vector  $V$ ; the  $n_X \times n_V$  stoichiometric matrix  $N$  relates the rate of change  $\dot{X}$  of  $X$  to  $V$  by Equation (1) repeated here:

$$\dot{X} = NV \quad (2.1)$$

The elements of  $N$  are integers that determine the amount of each species participating in the reaction. For example, the reaction  $A + B \xrightleftharpoons{r} C + D$  of Figure 11 can be represented by Equation (1) where:

$$X = (x_A \ x_B \ x_C \ x_D)^T \quad N = (-1 \ -1 \ 1 \ 1)^T \quad V = v_r$$

where  $x_A$  is the molar amount of substance  $A$  etc and  $v_r$  is the reaction flow.

As discussed in the basic textbooks (for example that of Klipp et al. [8]), the mathematical concept of a *null space* of  $N$  gives useful information about the fundamental properties of the biomolecular system described by  $N$ . These are two null spaces: the left null space described by the matrix  $G$  where  $GN = 0$  and the right null space described by the matrix  $K_p$  where  $NK_p = 0$ . In the case of the open systems discussed in § 2,  $N$  is replaced by  $N^{cd}$ .

The significance of  $G$  is that pre-multiplying both sides of Equation (1) by  $G$  gives

$$G\dot{X} = GNV = 0$$

Hence the linear combinations of  $X$  implied by the rows of  $G$  are *constant*; in systems biology nomenclature such combinations are known as *conserved moieties*. In case of the example system, one possible matrix  $G$  is:

$$G = \begin{pmatrix} 1 & 0 & 1 & 0 \\ 1 & 0 & 0 & 1 \\ 0 & 1 & 1 & 0 \end{pmatrix}$$

It can be verified that  $GN = 0$  and the corresponding three conserved moieties are

$$x_A + x_C \qquad x_A + x_D \qquad x_B + x_C$$

The significance of  $K_p$  is that if the elements of  $V$  are not independent but rather defined by  $V = K_p v$  then Equation (1) gives

$$\dot{X} = NK_p v = 0$$

Hence the columns of  $K_p$  determine *pathways*: combinations of non zero flows which lead to constant species amounts. In this example, there is no  $K_p$  such that  $NK_p = 0$ . However, in the special case that the four species  $A - D$  are *chemostats* (their values are held constant by some external flows) then  $N$  now has four *zero* entries and  $K_p = 1$  and thus the four species have constant amounts for any  $v$  and thus the single reaction  $r$  trivially becomes a pathway. As discussed in the paper, the more complex systems of Figures 1, 3 & 8 have non-trivial pathways.

Neither  $G$  nor  $K_p$  are unique. The seminal contribution discussed by Heinrich and Schuster [5] was to examine the case where the entries of  $K_p$  are both *integer* and *non-negative* thus defining pathways where all reaction flows have the same sign and are integer multiples of some base flows. This idea forms the basis of analysing large-scale biomolecular systems by *flux-balance analysis* (FBA) [8]. Together with the bond graph concepts outlined in § A, this idea provides the foundation for this paper.